ELSEVIER

Journal of Power Sources 108 (2002) 192–203

JOURNAL OF POWER SOURCES

www.elsevier.com/locate/jpowsour

A new semi-empirical approach to performance curves of polymer electrolyte fuel cells

L. Pisani, G. Murgia, M. Valentini, B. D'Aguanno*

Center for Advanced Studies, Research and Development in Sardinia, Uta (CA), Italy

Received 15 September 2001; received in revised form 22 December 2001; accepted 2 January 2002

Abstract

We derive a semi-empirical equation to describe the performance curves of polymer electrolyte membrane fuel cells (PEMFCs). The derivation is based on the observation that the main non-linear contributions to the cell voltage deterioration of H_2/air feed cells are deriving from the cathode reactive region. To evaluate such contributions we assumed that the diffusion region of the cathode is made by a network of pores able to transport gas and liquid mixtures, while the reactive region is made by a different network of pores for gas transport in a liquid permeable matrix. The mathematical model is largely mechanistic, with most terms deriving from phenomenological mass transport and conservation equations. The only full empirical term in the performance equation is the Ohmic overpotential, which is assumed to be linear with the cell current density. The resulting equation is similar to other published performance equations but with the advantage of having coefficients with a precise physical origin, and a precise physical meaning. Our semi-empirical equation is used to fit several set of published experimental data, and the fits showed always a good agreement between the model results and the experimental data. The values of the fitting coefficients, together with their associated physical meaning, allow us to asses and quantify the phenomenology which is set on in the cathode as the cell current density is increased. More precisely, we observe the development of the flooding and of the local decrease of the oxygen concentration. Further developments of such a model for the cathode compartment of the fuel cell are discussed.

Keywords: PEMFC; Semi-empirical approach; Mass transport

1. Introduction

The last decade saw an explosion in the number of papers dealing with the modelling of fuel cells, and in particular with the modelling of polymer electrolyte membrane fuel cells (PEMFCs). For what concerns the spatial dimensionality, published models include 0D models [1–6], in which no spatial dimensions of the cell are explicitly taken into account, 1D models [7–11], in which the spatial dimension entering into the description is the one perpendicular to the plates of the cell, and 2D models [12–15], in which the considered planes are those perpendicular to the cell plates. To our knowledge, 3D models in which the single cell is considered in its full glory have been only published for solid oxide fuel cells [16]. For what concerns the temporal dimensionality, both steady-state and dynamical models already appeared. While for what concerns the included phenomenology, the larger amount of published models deals with charge and mass transport and conservation. Few also include heat transport.

Clearly, the complexity of the models is extremely variable, and it goes from the one-equation approach typical of the empirical models, to very intimidating set of coupled differential equations with tens of spatial-dependent material properties. It is believed that the pay back of complex models is a strong increase in their predictive power. However, and before to develop new complex approaches, it is always better to fully exploit the potentialities of more simple point of view.

An open problem of simple empirical approaches which try to mimic the performance curve of PEMFC is the physical origin and meaning of the cell current-dependent terms. This is true for some of the most spread-out performance equations which are that of Kim et al. [1]

$$V_{\text{cell}} = E_{0,\text{K}} - R_{\text{cell,K}} I - b_{\text{K}} \ln(I) - m_{\text{K}} \exp(n_{\text{K}} I), \tag{1}$$

that of Lee et al. [2]

$$V_{\text{cell}} = E_{0,\text{L}} - R_{\text{cell,L}} I - b_{\text{L}} \ln(I) - m_{\text{L}} \exp(n_{\text{L}} I) - a_{\text{L}} \ln(P/P_{\text{O}_2}), \tag{2}$$

* Corresponding author. Tel.: +39-70-2796-250; fax: +39-70-2796-216.
E-mail address: bruno@crs4.it (B. D'Aguanno).

0378-7753/02/$ – see front matter
PII: S0378-7753(02)00014-9

Nomenclature

a	effective catalyst area per unit volume
c_{O_2}	concentration of oxygen
C_D	cathode diffusion region
C_R	cathode reaction region
D_{i-j}	diffusion coefficient of the pair i–j in a gas binary mixture
D_{O_2}	diffusion coefficient of oxygen
D_p	mean pore–pore distance
F	Faraday constant
i	ionic current density
i_0	exchange current density
I	cell current density
K	proportionality constant
K_h	Henry's law constant
L	diffusion length of oxygen
L_c	characteristic diffusion length
L_l	longitudinal diffusion length
L_p	mean pore length
L_t	transversal diffusion length
M	membrane region
N_d	diffusion mechanism parameter
N_{O_2}	mass flux of oxygen
P	hydraulic pressure
R	gas constant
R_{cell}	cell resistence
R_p	mean pore radius
s_e	number of electrons exchanged in the electrochemical reaction
S	flooding parameter
T	temperature
V_{cell}	cell potential
V_{C_R}	volume of C_R region
x_i	molar fraction of species i

Greek letters

α_a	anode transfer coefficient
α_c	cathode transfer coefficient
β_F	Faraday constant in units of RT
ϵ_g	gas porosity
γ	kinetic exponent of the species in the Butler–Volmer equation
η	overpotential
ϕ_l	electric potential of the liquid phase
ϕ_s	electric potential of the solid phase
μ	empirical constant
σ	area crossed by oxygen to make its electrochemical reaction
σ_c	cross-area of the cell
Ξ	integrated oxygen concentration

Subscripts

int	interface value
Ohm	Ohmic value
ref	at the reference state
w	water

Superscripts

0	value at the zero-current density
eff	effective in porous media
l	value at the limiting current density

and that of Squadrito et al. [3]

$$V_{cell} = E_{0,S} - R_{cell,S}I - b_S \ln(I) + a_S I^k \ln(1 - \beta I). \quad (3)$$

Here, V_{cell} is the cell potential, I the cell current density, P the pressure, and all the other quantities are the fitting coefficients.

Since all these equations are rich of fitting coefficients, they always reproduce experimental data in an accurate way. However, very little is learned about the phenomena which take place in the cell as the cell current, I, changes. In addition, the systematic application of these equations does not show clear trends in the fitting coefficients, eliminating the possibility of using them as predictive tools.

To repair this state of affair, Amphlett and coworkers [4–6] made a semi-empirical derivation of a performance equation, in which both mechanistic and empirical features are present in the fitting coefficients. However, the proposed equation shows some lacks in reproducing experimental data, especially at high current density.

In the same spirit, we also present a semi-empirical derivation of a performance equation with the goal of having the largest number of mechanistic derived coefficients. The hope is that once the equation is used to fit experimental data, the values of the mechanistic derived coefficients will give us information on the phenomena which are set on in the cell as the current is changed.

To make the semi-empirical derivation of the performance equation, we pay attention to transport cathode phenomena by introducing a porous structure in both the diffusion and reactive regions of the cathode itself. This choice is made to introduce into the model flooding and concentration effects, which severely affect the fuel cell behavior at high cell current density.

After an introductory and qualitative analysis of performance curve made in Section 2, Section 3 of this paper is devoted to the development of our model. Section 4 shows comparisons with other published performance equations, with experimental data, and with some of the published mechanistic models, too. Section 5, contains summary and conclusions.

2. Qualitative analysis of performance curves

Potential losses inside a fuel cell originate either at the interfaces between solid and fluid phase, where all the electrochemistry takes place, or internally to each single

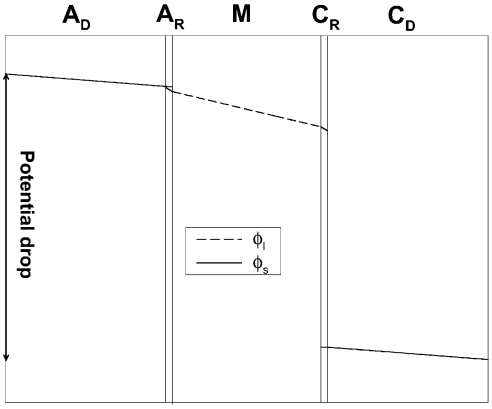

Fig. 1. Typical cell potential drop within the different regions of a PEMFC at a given cell current density. A_D, C_D: anode and cathode diffusion regions; A_R, C_R: anode and cathode reaction regions; M: membrane; ϕ_l, ϕ_s: liquid and solid phase potentials.

phase. The single phase losses are essentially of Ohmic origin, linear with the cell current density, I, and therefore, they have a trivial effect on the performance curves (cell voltage against cell current density). More complex is the I-behavior of the interface overpotentials which, as illustrated in Fig. 1, originate in the small electrode reactive regions where liquid phase and solid phase coexist.

Two main factors govern the magnitude of the interface overpotentials: the reaction kinetic and the local concentration or, in other words, the local availability of reactants.

As appear in Fig. 1, the anodic term is much smaller than the cathodic one. This is because of the extremely favorable electrochemical kinetic constant associated with the hydrogen reaction as compared to that of the oxygen reaction, and because hydrogen supply do not present problems. Indeed, hydrogen is supplied as pure H_2 (or with small concentrations of contaminants), while oxygen is mostly supplied as air. Furthermore, flooding of the diffusive regions is more severe in the cathode than in the anode, because liquid water is generated during the cathode reaction.

The above discussion is also well illustrated by Fig. 2 which shows typical results obtained from simulation methods (in this case, results are from the modified Bernardi–Verbrugge model [8,9]). The contributions of the different regions of the PEMFC to the cell potential, V_{cell}, are now plotted as a function of the cell current density, I. It is seen that the main non-linear contribution comes from the cathode reactive region, C_R, which accounts for both the activation and concentration overpotentials.

Therefore, we write the cell potential as made up of a zero-current term, $E(I=0)$, MEA potential drop terms of Ohmic origin, $\eta^{\alpha}_{\text{Ohm}}(I)$, and potential drop terms originated by the interface electrochemistry in the anode and cathode reactive regions, $\eta^{\alpha}_{\text{int}}(I)$:

$$V_{\text{cell}}(I) = E(I=0) + \eta^{\text{A}}_{\text{Ohm}}(I) + \eta^{\text{C}}_{\text{Ohm}}(I) + \eta^{\text{M}}_{\text{Ohm}}(I) + \eta^{\text{A}}_{\text{int}}(I) + \eta^{\text{C}}_{\text{int}}(I), \quad (4)$$

and we restrict our analysis to the $\eta^{\text{C}}_{\text{int}}(I)$ term by rewriting $V_{\text{cell}}(I)$ as

$$V_{\text{cell}}(I) \simeq E(I=0) - R_{\text{cell}} I + \eta^{\text{C}}_{\text{int}}(I). \quad (5)$$

Extension of the analysis to $\eta^{\text{A}}_{\text{int}}(I)$ can be done by following the same lines with only minor changes.

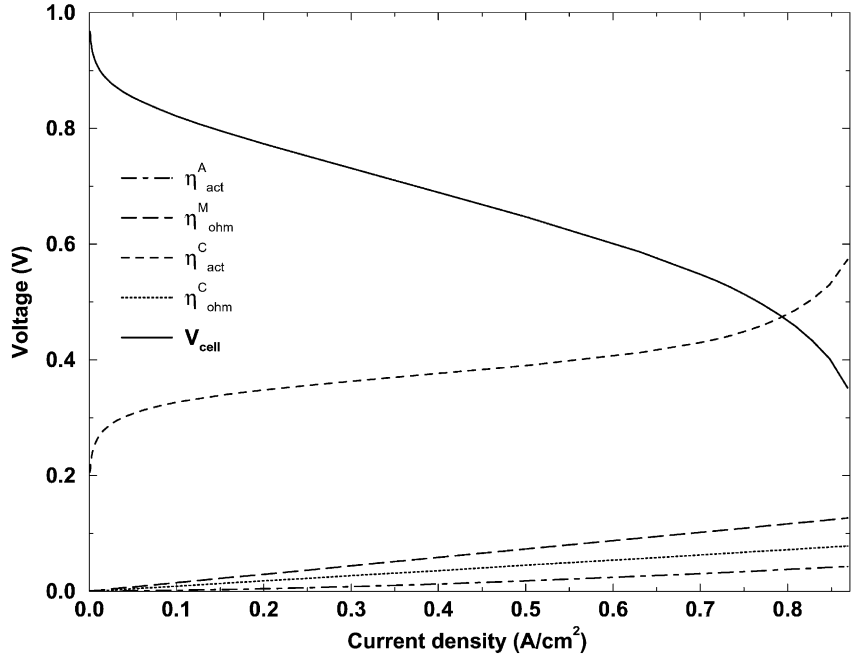

Fig. 2. Performance curve and cell overpotentials.

3. The semi-empirical approach

To relate the interphase cathodic overpotential, $\eta_{\text{int}}^{\text{C}}(I)$, to the cell current density, I, we start from the Butler–Volmer equation

$$\nabla \cdot i = a i_{0,\text{ref}} \left(\frac{c_{\text{O}_2}(z)}{c_{\text{O}_2,\text{ref}}} \right)^{\gamma} \left[\text{e}^{\alpha_a \beta_{\text{F}} (\phi_s(z) - \phi_l(z))} - \text{e}^{-\alpha_c \beta_{\text{F}} (\phi_s(z) - \phi_l(z))} \right], \tag{6}$$

where i is the ionic current density, a the effective catalyst area per unit of volume, $i_{0,\text{ref}}$ the exchange current density, c_{O_2} the oxygen concentration, γ a kinetic coefficient, α_i the electrode transfer coefficients, and β_{F} the Faraday constant in units of RT.

The values taken by ϕ_s and ϕ_l within the region C_R (see Fig. 1) indicate that the first exponential of Eq. (6) (the anode semi-reaction) is completely negligible, and that the potential variations of Ohmic origin are negligible, too, due to the small dimensions of the region. Within a good approximation, Eq. (6) can be re-written as

$$\nabla \cdot i \approx -a i_{0,\text{ref}} \left(\frac{c_{\text{O}_2}}{c_{\text{O}_2,\text{ref}}} \right)^{\gamma} \text{e}^{-\alpha_c \beta_{\text{F}} \eta_{\text{int}}^{\text{C}}}, \tag{7}$$

where $\eta_{\text{int}}^{\text{C}}$ is defined as

$$\eta_{\text{int}}^{\text{C}} = \phi_s^{\text{C}_\text{R}/\text{C}_\text{D}} - \phi_l^{\text{C}_\text{R}/\text{C}_\text{D}}. \tag{8}$$

The integration of the Butler–Volmer equation over the cathode reactive region gives the total amount of current produced in the cell, i.e. the cell current density I. Then, by integrating Eq. (7) in C_R we get

$$\sigma_c I = \int_{\text{C}_\text{R}} \nabla \cdot i \, \text{d}V \approx -\frac{a i_{0,\text{ref}}}{c_{\text{O}_2,\text{ref}}^{\gamma}} \text{e}^{-\alpha_c \beta_{\text{F}} \eta_{\text{int}}^{\text{C}}} \int_{\text{C}_\text{R}} c_{\text{O}_2}^{\gamma} \, \text{d}V, \tag{9}$$

in which, σ_c is the cross-area of the cell.

From Eq. (9) and by throwing all the constant terms in a generic constant K, we get for $\eta_{\text{int}}^{\text{C}}(I)$ the expression

$$\eta_{\text{int}}^{\text{C}}(I) = K - \frac{1}{\alpha_c \beta_{\text{F}}} [\ln(I) - \ln(\Xi(I))], \tag{10}$$

where we have defined

$$\Xi(I) = \int_{\text{C}_\text{R}} (c_{\text{O}_2}(I))^{\gamma} \, \text{d}V. \tag{11}$$

At this point, the problem is shifted to the finding of an expression for $\Xi(I)$. This is done in two steps. First, $\Xi(I)$ is expressed as a function of the interface concentration $c_{\text{O}_2}^{\text{C}_\text{R}/\text{C}_\text{D}}(I)$. Second, an expressions for $c_{\text{O}_2}^{\text{C}_\text{R}/\text{C}_\text{D}}(I)$ is found. The first step involves the mechanisms of oxygen diffusion inside the C_R region, while the second step concerns oxygen diffusion in the C_D region. Because $\Xi(I)$ in Eq. (10) is inside a logarithm, all the multiplying factors which do not depend on I (including numerical factors, physical constants, measure units, etc.) can be thrown away in the trashcan constant K, and we can proceed by proportionality relations.

3.1. Total oxygen concentration

In the reactive region, the material conservation equation for oxygen reads as $\nabla \cdot N_{\text{O}_2} \propto \nabla \cdot i$. Such an equation can be integrated in C_R, and by using the condition of negligible oxygen flux at $\text{M}/\text{C}_\text{R}$ interface and the first equality in Eq. (9), we have $\sigma |N_{\text{O}_2}^{\text{C}_\text{R}/\text{C}_\text{D}}| \propto \sigma_c I$. By using this result and the phenomenological diffusion equation, $N_{\text{O}_2} = -D_{\text{O}_2} \nabla c_{\text{O}_2}$, the gradient of the oxygen concentration at the $\text{C}_\text{R}/\text{C}_\text{D}$ interface becomes

$$|\nabla c_{\text{O}_2}|_{\text{C}_\text{R}/\text{C}_\text{D}} \propto \frac{I}{\sigma}. \tag{12}$$

Here, we made explicit the dependence on σ, which is the surface crossed by oxygen to make its electrochemical reaction, since it can change according to the physical model chosen to describe oxygen diffusion within the reactive region.

By assuming a linear decrease of the oxygen concentration profile within the C_R region, the length $L(I)$ over which oxygen can diffuse (i.e. the distance over which $c_{\text{O}_2}(I) \neq 0$) is defined as

$$L(I) = \frac{c_{\text{O}_2}^{\text{C}_\text{R}/\text{C}_\text{D}}(I)}{|\nabla c_{\text{O}_2}(I)|_{\text{C}_\text{R}/\text{C}_\text{D}}} \propto \sigma \frac{c_{\text{O}_2}^{\text{C}_\text{R}/\text{C}_\text{D}}(I)}{I}, \tag{13}$$

where we also made use of Eq. (12).

Now, to evaluate the volume integral of the linear function

$$c_{\text{O}_2}(l, I) = \begin{cases} c_{\text{O}_2}^{\text{C}_\text{R}/\text{C}_\text{D}}(I)(1 - l/L(I)) & \text{for} \quad l < L(I), \\ 0 \quad \text{for} \quad l > L(I), \end{cases} \tag{14}$$

over the C_R region, we need a physical model which gives us a geometrical expression for the incremental volume $\text{d}V$ and for the integration domain. In general, given a model for the region C_R, a characteristic length L_c can be defined such that when $L(I) > L_c$ oxygen pervades the whole region while when $L(I) < L_c$ this would not happen. Then two diffusion regimen can be recognized:

1. for $L(I) \gg L_c$, the oxygen concentration profile is nearly flat and we have $\Xi(I) = (c_{\text{O}_2}^{\text{C}_\text{R}/\text{C}_\text{D}}(I))^{\gamma} V_{\text{C}_\text{R}}$;
2. for $L(I) < L_c$, oxygen diffusion is limited; the integral must be explicitly calculated and depends on the physical model.

Many mechanistic models found in the literature propose a uniform C_R region and no limitations for the oxygen diffusion. Within these models, the characteristic length is the C_R thickness, L_{C_R}.

A more realistic model of the reactive region, C_R, results if we consider gas pores going through the region, and both longitudinal (1D) gas-phase and transversal (2D) liquid phase oxygen diffusion mechanisms. For this model, we have two characteristic lengths: the mean pore length (L_p) which characterizes the longitudinal diffusion and the mean pore–pore distance (D_p) which characterizes the transversal diffusion.

Table 1
Oxygen concentration integrals for different diffusion mechanisms

Model	Limited diffusion mechanisms	Conditions	Integral	N_d
Homogeneous		$L \gg L_{C_R}$	$(c_{O_2}^{C_R/C_D}(I))^\gamma$	0
		$L < L_{C_R}$	$\frac{c_{O_2}^{C_R/C_D}(I)}{I}(c_{O_2}^{C_R/C_D}(I))^\gamma$	1
Pore gas	None	$L_l \gg L_p$ $L_t \gg D_p$	$(c_{O_2}^{C_R/C_D}(I))^\gamma$	0
	Longitudinal	$L < L_p$	$\frac{c_{O_2}^{C_R/C_D}(I)}{I}(c_{O_2}^{C_R/C_D}(I))^\gamma$	1
	Transversal	$L < D_p$ $L \gg R_p$	$\left(\frac{c_{O_2}^{C_R/C_D}(I)}{I}\right)^2(c_{O_2}^{C_R/C_D}(I))^\gamma$	2
		$L < D_p$ $L \ll R_p$	$\frac{c_{O_2}^{C_R/C_D}(I)}{I}(c_{O_2}^{C_R/C_D}(I))^\gamma$	1
	Both	$L_t < D_p$ $L_t \gg R_p$ $L_l < L_p$	$\left(\frac{c_{O_2}^{C_R/C_D}(I)}{I}\right)^5(c_{O_2}^{C_R/C_D}(I))^\gamma$	5
		$L_t < D_p$ $L_t \ll R_p$ $L_l < L_p$	$\left(\frac{c_{O_2}^{C_R/C_D}(I)}{I}\right)^3(c_{O_2}^{C_R/C_D}(I))^\gamma$	3

In the Appendix A, the value of $\Xi(I)$ is estimated for the homogeneous and gas pores models. Within the latter model the cases where only longitudinal, only transversal or both diffusion mechanisms are limited are taken into account. The results are summarized in Table 1. It is seen that in all the considered cases, the value of $\Xi(I)$ can be expressed as

$$\Xi(I) \propto (c_{O_2}^{C_R/C_D}(I))^\gamma \left(\frac{c_{O_2}^{C_R/C_D}(I)}{I}\right)^{N_d(I)}, \quad (15)$$

which is the searched equation.

The values of the parameter $N_d(I)$, give indication on the oxygen diffusion mechanism which is set on at a given cell current density. Note that most of the cases presented in Table 1 (specially the cases with the conditions ≪and≫), correspond to border-line regimens. At intermediate conditions, transition regimens join smoothly the border-line ones.

3.2. Interface oxygen concentration

To express the oxygen concentration at the C_R/C_D interface as a function of the current density, we model the gas diffusion through the pores of the cathode diffusion region with the Stefan–Maxwell equations

$$\nabla x_i = \sum_{j=1}^{n} \frac{RT}{PD_{i-j}^{eff}}(x_i N_j - x_j N_i) \quad i = N_2, w, O_2, \quad (16)$$

where D_{i-j}^{eff} is an effective $i-j$ pair diffusion coefficient in the porous medium, N_i the molar flux of species i, and x_i its molar fraction.

By following the derivation of [8], which is based on the assumptions that both the flux of nitrogen, N_{N_2}, and the gradient of water concentration, ∇x_w, are zero, Eq. (16) gives for the gradient of nitrogen concentration the expression

$$\frac{P}{RT}\nabla x_{N_2} = x_{N_2} N_{O_2,g}\left[\frac{1}{D_{N_2-O_2}^{eff}} + \frac{x_w}{x_{O_2}D_{w-N_2}^{eff} + x_{N_2}D_{w-O_2}^{eff}}\right]. \quad (17)$$

By knowing that $D_{w-N_2}^{eff} \approx D_{w-O_2}^{eff}$ [17], that the O_2 flux is related to the cell current, $N_{O_2,g} = I/(s_e F)$, and that the effective diffusion depends on the gas-phase volume fraction, $D_{i-j}^{eff} = D_{i-j}\epsilon_g^\mu$ [9], Eq. (17) can be written as

$$\nabla x_{N_2} = x_{N_2}\frac{A}{\epsilon_g^\mu} I, \quad (18)$$

where the constant term A is

$$A = \frac{RT}{s_e F}\left[\frac{1}{PD_{N_2-O_2}} + \frac{x_w}{(1-x_w)PD_{w-N_2}}\right]. \quad (19)$$

In these relations s_e is the number of electrons exchanged in the electrochemical reactions, μ is an empirical constant [9], and D_{i-j} the pair diffusion coefficients in a non-porous medium.

When ϵ_g is z-independent, the differential equation (18) can be solved to give

$$x_{N_2}^{C_R/C_D} = x_{N_2}^0 \exp\left(\frac{AL}{\epsilon_g^\mu} I\right), \quad (20)$$

where L is the thickness of the diffusive region and the zero of the z-coordinate is fixed at the C_F/C_D interface.

From the relation $x_{O_2} + x_{N_2} = 1 - x_w$, which is constant through the gas pores of the cathode, Eq. (20) can be rewritten for $x_{O_2}^{C_R/C_D}$ as

$$x_{O_2}^{C_R/C_D} = x_{O_2}^0 - x_{N_2}^0 \left[\exp\left(\frac{AL}{\epsilon_g^\mu} I \right) - 1 \right]. \tag{21}$$

From this relation we see that at $I = 0$, $x_{O_2}^{C_R/C_D} = x_{O_2}^0$, and that the limiting current I_l, i.e. the current density value at which the oxygen concentration $x_{O_2}^{C_R/C_D} = 0$ is

$$I_l = \ln\left(1 + \frac{x_{O_2}^0}{x_{N_2}^0} \right) \frac{\epsilon_g^\mu(I_l)}{AL}, \tag{22}$$

where we made the important step of having the gas porosity ϵ_g as a function of the current density I.

Finally, and by knowing that at the C_R/C_D interface the dissolved-oxygen concentration in the membrane phase is related to the gas-phase molar fraction by the Henry's law constant K_h

$$\frac{K_h}{P} c_{O_2}^{C_R/C_D} = x_{O_2}^{C_R/C_D}, \tag{23}$$

we can write for $c_{O_2}^{C_R/C_D}(I)$ the expression

$$c_{O_2}^{C_R/C_D}(I) = c_{O_2}^{C_R/C_D}(0) \left(1 - \frac{x_{N_2}^0}{x_{O_2}^0} \left[\left(1 + \frac{x_{O_2}^0}{x_{N_2}^0} \right)^{I/I_l(\epsilon_g(I_l)/\epsilon_g(I))^\mu} \right] \right). \tag{24}$$

For small inlet oxygen–nitrogen mole ratio, first-order expansion gives the simpler expression

$$c_{O_2}^{C_R/C_D}(I) = c_{O_2}^{C_R/C_D}(0) \left[1 - \frac{I}{I_l} \left(\frac{\epsilon_g(I_l)}{\epsilon_g(I)} \right)^\mu \right]. \tag{25}$$

To characterize the concentration functions (24) and (25), we analyze two elementary functions for $\epsilon_g(I)$.

1. The exponential function

$$\epsilon_g(I) = \epsilon_g^l S^{(1-I/I_l)} \begin{cases} = \epsilon_g^0 & \text{for} \quad I = 0, \\ = \epsilon_g^l & \text{for} \quad I = I_l, \\ = 0 & \text{for} \quad I = \infty. \end{cases} \tag{26}$$

2. The linear function

$$\epsilon_g(I) = \epsilon_g^0 + \frac{I}{I_l}(\epsilon_g^l - \epsilon_g^0) \begin{cases} = \epsilon_g^0 & \text{for} \quad I = 0, \\ = \epsilon_g^l & \text{for} \quad I = I_l. \end{cases} \tag{27}$$

In both cases, ϵ_g^0 is a physical parameter which depends on the preparation of the diffusion part of the MEA, while ϵ_g^l and I_l are parameters which characterize the flooding process. Eq. (22) links ϵ_g^l with I_l, therefore, we have just one independent parameter.

To study the behavior of Eq. (24) with $\epsilon_g(I)$ given by the exponential and linear function, we fix $I_l = 1$, $c_{O_2}^{C_R/C_D}(0) = 1$, $\mu = 1.5$ from [9] and the inlet oxygen nitrogen mole ratio to 0.27 which corresponds to air feeding, and variate the parameter S.

In Fig. 3A, exponential and linear porosity functions are inserted into Eq. (24) and compared for two different values of S. In addition, the exponential porosity function is inserted into the approximate Eq. (25) and plotted as well.

The case $S = 1$ ($\epsilon_g^l = \epsilon_g^0$) corresponds to the case where there is no flooding; in this case, the two curves coming from expression (24) coincide and are nearly linear. From the figure, we see that the qualitative behavior of the three functions while changing S is the same. This is even more evident when we look at the logarithms of the same functions (Fig. 3B) which is the function we need in our relations (see Eq. (10)). Notice, however, that the choice of the porosity function brings slight changes in the value of S. In conclusion, we can select arbitrarily one of the three expressions but bearing in mind that the value of S is not strictly quantitative. By using a simplicity criterion, we

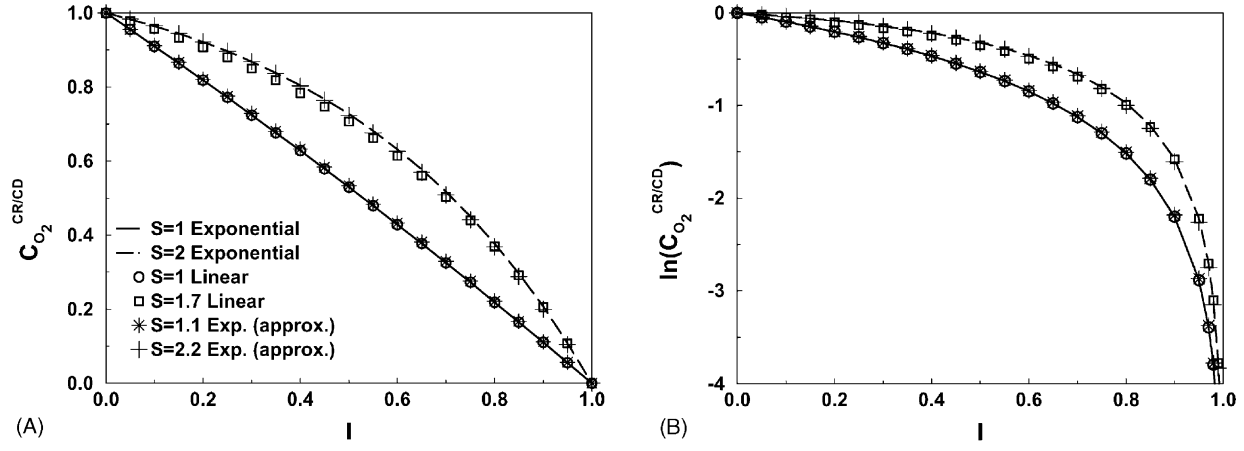

Fig. 3. Oxygen concentration with different porosity functions.

choose the exponential porosity function, and Eq. (25) becomes

$$c_{O_2}^{C_R/C_D}(I) = c_{O_2}^{C_R/C_D}(0)\left[1 - \frac{I}{I_l} S^{\mu((I/I_l)-1)}\right]. \quad (28)$$

3.3. The semi-empirical equation

The results of the previous subsections are now inserted into Eq. (10). By first using the results of Eq. (15), we get

$$\eta_{int}^{C} = K - \frac{1}{\alpha_c \beta_F}\left[(1 + N_d(I))\ \ln(I) - (\gamma + N_d(I))\ \ln(c_{O_2}^{C_R/C_D}(I))\right]. \quad (29)$$

The first term of this equation is dominant at low current densities and gives an expression for the activation overpotential, while the second term becomes dominant where the oxygen concentration is small and expresses the concentration overpotential. It follows that when this equation is used as a fitting equation, the coefficient value of the first logarithm term in the square brackets will be extracted from the experimental behavior at low I, while that of the second logarithm term from the experimental behavior at high I. For this reason, we reduce the continuous I dependence of N_d to two limiting values, one at low I, N_d^0, and one at high I, N_d^l, and write η_{int}^{C} as

$$\eta_{int}^{C} = K - \frac{1}{\alpha_c \beta_F}\left[(1 + N_d^0)\ \ln(I) - (\gamma + N_d^l)\ \ln\left(1 - \frac{I}{I_l} S^{-\mu(1-I/I_l)}\right)\right], \quad (30)$$

in which we also made use of expression (28).

Finally, the cell potential, Eq. (5), becomes

$$V_{cell} \simeq E_0 - R_{cell} I - b\ \ln(I) + a\ \ln\left(1 - \frac{I}{I_l} S^{-\mu(1-I/I_l)}\right), \quad (31)$$

with

$$E_0 = E(I = 0) + K; \qquad b = \frac{1 + N_d^0}{\alpha_c \beta_F}; \qquad a = \frac{\gamma + N_d^l}{\alpha_c \beta_F}, \quad (32)$$

which is the main result of this section. In Eq. (31), all the I-dependent terms have a well precise origin, and all parameters have a specified physical meaning.

4. Comparisons between theory and experiments

The interest of a comparison between Eq. (31) and empirical equations as that of Kim et al. [1] or Squadrito et al. [3] is double. On one hand, we gain a better insight on the empirical parameters by giving them a physical meaning; on the other hand, through the experimental values of the empirical parameters, we obtain indications on the values of the parameters N_d and S, which characterize the physical diffusion mechanisms inside the reactive and diffusive regions, respectively.

4.1. Analysis of empirical parameters

Let now compare our expression for the cell potential, Eq. (31), with the empirical equation given by Squadrito et al. [3] and Kim et al. [1]:

$$\begin{aligned} V_{cell} &= E_0 - R_{cell} I - b\ \ln(I) + a\ \ln\left(1 - \frac{I}{I_l} S^{-\mu(1-I/I_l)}\right) \quad \text{(this work)} \\ V_{cell} &= E_{0,S} - R_{cell} I - \frac{b_S}{\ln 10}\ \ln(I) + a_S I^k\ \ln(1 - \beta I) \quad \text{(Squadrito)} \\ V_{cell} &= E_{0,K} - R_{cell} I - \frac{b_K}{\ln 10}\ \ln(I) - m \exp(nI) \quad \text{(Kim)} \end{aligned} \quad (33)$$

The equation of Squadrito et al. [3] fits quite well our equation. The only apparent difference is in the shape of the concentration overpotential (last logarithm term on the right side).

To find correspondences, in Fig. 4, we plot the argument of the second logarithm term of the Squadrito relation

$$f(I) = (1 - \beta I)^{a_S I^k}, \quad (34)$$

for $\beta = 1/I_l = 1$, $a_S = (0.85/I_l)^k$, and different values of k. For such parameter values, we notice that the functional form of the curves in this figure compares very well with that of the curves of Fig. 3A. This similarity, leads us to interpret the k parameter in terms of the water flooding phenomena: $k = 0$ corresponds to $S = 1$ which means the absence of water flooding, while $k > 0$ corresponds to $S > 1$ (i.e. $\epsilon_g^l < \epsilon_g^0$), which in turn means that water flooding reduced the gas porosity. The similarity also allows us to define a rescaled quantity $a'_S = (I_l/0.85)^k a_S$ which now corresponds to our a parameter.

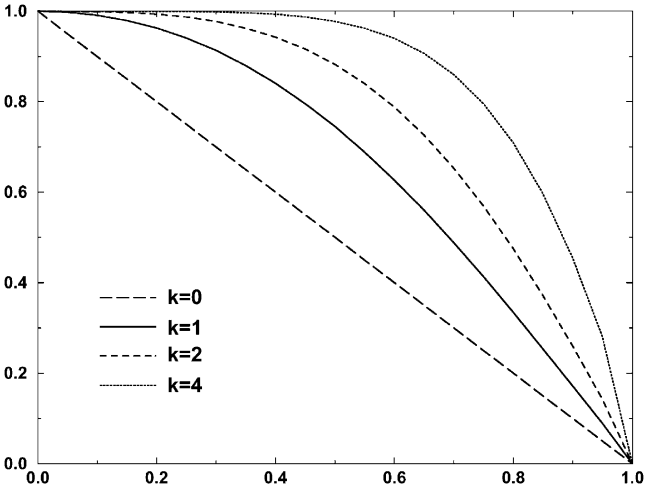

Fig. 4. $f(I)$ at different values of the k parameter.

Table 2
Values of the parameters given in Eq. (32) and needed to fit the Squadrito et al. [3] experimental data

Membrane	Temperature (°C)	Gas pressures (bar)	E_0 (V)	R_{cell} (Ω/cm^2)	I_l (A/cm^2)	$b_S/\ln 10$ (V)	a'_S (V)	$a'_S \ln 10/b_S$
NF117	70	1/1	0.937	0.30	0.824	0.024	0.131	5.4
		1.5/1.5	0.936	0.28	0.880	0.026	0.144	5.5
		2.5/3	0.962	0.28	0.907	0.025	0.152	6.1
		3/5	0.970	0.24	0.962	0.026	0.179	6.9
NF115	70	1/1	0.933	0.24	0.810	0.025	0.099	4.0
		1.5/1.5	0.940	0.23	0.833	0.026	0.102	3.9
		2.5/3	0.956	0.25	0.923	0.023	0.080	3.5
NF112	70	2.5/3	0.946	0.19	1.006	0.022	0.062	2.8
NF117	80	3/5	0.961	0.28	0.965	0.023	0.112	4.9
NF115			0.966	0.23	0.972	0.022	0.077	3.5
NF112			0.955	0.18	1.008	0.021	0.070	3.3

Other links between Squadrito et al. [3] parameters and those appearing in our empirical equation can be found by comparing the terms with the same I-dependence type:

$$E_{0,S} = E(I=0) + K; \qquad \frac{b_S}{\ln 10} = \frac{1}{\alpha_c \beta_F}(1 + N_d^0);$$
$$k = S; \qquad \beta = \frac{1}{I_l}. \tag{35}$$

From the analysis done in the previous sections, it follows that k and β depend on the behavior of the oxygen concentration in the C_D region while b_S and a'_S depend on the diffusion mechanisms inside the C_R region.

Kim et al. [1] use the equation shown on the third subequation of Eq. (33)to characterize both cells with air and with pure oxygen feeding. Since our analysis is for cells with air feeding, it is not possible to justify the use, in this case, of their exponential term. The Kim exponential term could still be the correct term to describe the concentration overpotential for cells with pure oxygen feeding. However, to establish this point our analysis requires further extensions.

4.2. Comparisons with experimental data

We start this subsection by first analyzing the values of the fitting parameters determined by Squadrito et al. [3], in order to assess the phenomenology which is set on in the cell as the current density is increased.

Table 2 reports the parameters obtained by fitting a number of experimental polarization curves in different conditions of hydrogen/air pressure, membrane thickness and temperature. The table shows the same data as in Table 3 of [3], with the values of the parameters b and a extracted from those of b_S and a_S (see Eqs. (32) and (35).

Squadrito et al. found for the k parameter a range of values between 2 and 4 in the 90% of fitted cases (for the fitting curves of Table 2, k is fixed to 3). This means that flooding phenomena are present, and that they reduce the porosity of the C_D region as the cell current density is increased.

To start to see if our semi-empirical analysis is consistent, we can use Eq. (22) to find the relation between S and I_l

$$S = \frac{\epsilon_g^0}{\epsilon_g^l} = \epsilon_g^0 \left(\frac{x_{O_2}^0}{x_{N_2}^0} \frac{1}{AL} \frac{1}{I_l} \right)^{1/\mu}. \tag{36}$$

The value of A, see Eq. (19), depends smoothly on temperature and at 70 °C is worth 0.37 cm/A; the rate between nitrogen and oxygen molar fraction in air is 3.76; the values of ϵ_g^0 and L depend on the particular preparation of the diffusion region, and Bernardi and Verbrugge [9] report $\epsilon_g^0 = 0.4$, $L = 0.026$ cm, and they also give $\mu = 1.5$. With these values and for $I_l = 0.9$ A/cm^2 (see Table 2), we get $S = 5.3$.

In Fig. 5, we compare the concentration profiles given by Eq. (34) for $k = 2$ and 4 with that given, for $S = 5.3$, by Eq. (28) and by the corresponding equation with the linear gas porosity, Eq. (27). We observe that both curves are consistent with the range of k, confirming the validity of the analysis about the physical meaning of the k parameter, and indicating that, at the limiting current, the gas porosity is reduced by about a factor of 5 with respect to its value at zero-current density.

Table 3
Fitting parameter for Eq. (31)

Gas pressures (bar)	O_2 (%)	E_0 (V)	R_{cell} (Ω/cm^2)	I_l (A/cm^2)	b (V)	N_d^l	S
1/1	27	0.933	0.21	0.816	0.026	3.0	5.7
2.5/3		0.956	0.225	0.928	0.023	2.5	5.2
1/1		0.940	0.26	0.763	0.027	7.5	5.9
1/3		0.982	0.26	1.070	0.028	5.5	4.7
1/5		0.996	0.29	1.149	0.027	5.5	4.5
1/1	20	0.917	0.38	0.789	0.020	4.5	5.5
	5	0.879	0.88	0.309	0.020	1.5	3.6

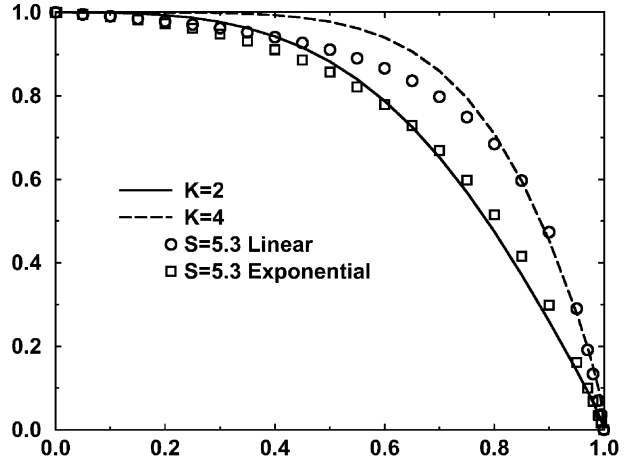

Fig. 5. Comparison between concentration profiles.

The last column of Table 2 shows the rates between the a and the b parameters. From Eq. (32), we have

$$\frac{a}{b} = \frac{\gamma + N_{\mathrm{d}}^{\mathrm{l}}}{1 + N_{\mathrm{d}}^{0}}. \tag{37}$$

Because the values found in literature for γ are in the range 0.5–1, we get agreement with the experimental data for $N_{\mathrm{d}}^{0} = 0$ and $N_{\mathrm{d}}^{\mathrm{l}}$ in the range 2–5. As it is clear from Eq. (13), at very low I the diffusion oxygen length becomes very large, and the reactive region is fully permeated by the oxygen molecules, $V_{\mathrm{eff}} = V_{\mathrm{C_R}}$. The choice of the fitting value $N_{\mathrm{d}}^{0} = 0$ is then perfectly justified (see Table 1, ''none'' case).

Instead, the range of $N_{\mathrm{d}}^{\mathrm{l}}$ values tells us that at high I the diffusion oxygen length becomes smaller than the characteristic lengths of the $\mathrm{C_R}$ porous region, and the oxygen molecules are unable to permeate all $V_{\mathrm{C_R}}$: concentration overpotetial is set on. Once more, the fitting values of $N_{\mathrm{d}}^{\mathrm{l}}$ are justified by our model. We then believe that the diffusion oxygen phenomenology, on which our model as been constructed, is substantially correct.

The last information we can extract from Table 2 is on the value of the cathodic transfer coefficient α_{c}. Indeed, once the diffusion model is defined, the values of N_{d} are known, and from the third sub-equation of Eq. (35), we can determine the value of the cathodic transfer coefficient α_{c}. A value of $N_{\mathrm{d}}^{0} = 0$ would mean α_{c} in the range 1.1–1.4 which seems to indicate a two electron rate determining step for the cathodic reaction.

Finally, we use our Eq. (31) as an ordinary semi-empirical equation to fit experimental polarization curves. The value of N_{d}^{0} has been fixed to 0 and S has been linked to I_{l} through Eq. (36).

In Fig. 6, we show the comparison between experimental data and fitted polarization curves. The experimental data of Fig. 6A are generated by inserting the fitting parameters reported in Table 3 of Squadrito et al. [3] into the corresponding empirical equation, which is given in the second sub-equation of Eq. (33). The experimental data of Fig. 6B and C are obtained through the same procedure but using the fitting data of Tables 2 and 3 of Kim et al. [1] and the fitting equation in the third sub-equation of Eq. (33). The experiments of Fig. 6A and B are performed at 70 °C and with a Nafion® 117 membrane, while the experiments of Fig. 6C are performed at 60 °C and with an Asahi Chemical Aciplex-S membrane. A good agreement between experimental data and our fitting results is found in all three cases.

Table 3 gives the values of the fitting parameters. The value of S is shown even if is not an independent parameter because of its physical meaning. The behaviour of S fits very well with what we expect about the water flooding phenomena. Indeed, by increasing the gas pressure, from simple arguments of capillarity, we expect that water would find a larger resistance to flooding and we observe, as expected, a decline of S [22]. Furthermore, the net decrease of S observed when the oxygen percentage drops from 20 to 5, is easily related to the corresponding fall of the limiting current: by decreasing the current density the water generated in the cathode reactive region decreases as well; this generates a pressure drop, and the flooding is also expected to decrease.

The observed fall of $N_{\mathrm{d}}^{\mathrm{l}}$ when the oxygen percentage drops from 20 to 5, is a very encouraging indication of the validity of its physical interpretation. Indeed, by following the same arguments expressed after Eq. (29), it appears evident that when I_{l} approaches 0, also $N_{\mathrm{d}}^{\mathrm{l}}$ must approach N_{d}^{0}, and this is clearly confirmed by the results.

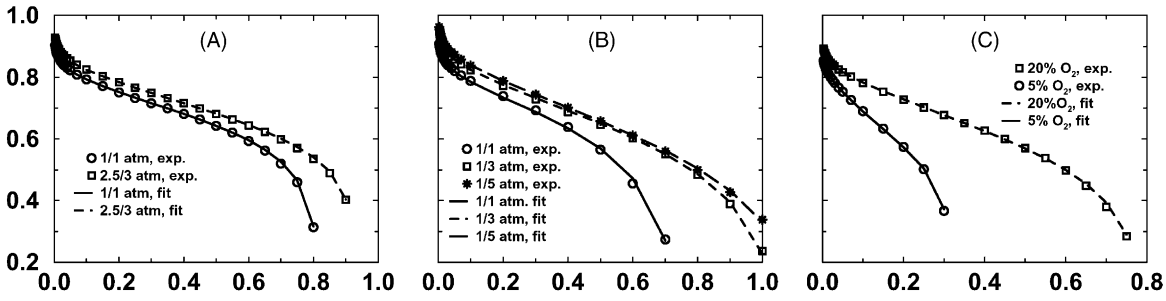

Fig. 6. Comparison between experimental data and theoretical results. Experimental data are from [3] (A), and from [1] (B and C).

However, the values of N_d appear to be slightly too high for the curves represented in Fig. 6B. There could be two reasons to explain this behavior:

1. We are not fitting directly experimental data but values which in turn are obtained by a fit of the experiments. It is quite likely that a high value of N_d is needed to represent the exponential fall which appears in the fitting expression (third sub-equation in Eq. (33)) used to represent the experimental data of cases B and C but not necessarily on the fall of the true experimental data.
2. We are considering the lack of oxygen due to the limited oxygen-in-nitrogen diffusion rate, as the only cause for the non-linear drop of the polarization curve at high current density. Fig. 10 and Table 3 of Kim et al. [1] (corresponding to case C) confirms this hypothesis; indeed the data obtained by using pure oxygen, and shown in the same figure, do not present any trace of non-linear drop. On the other hand, Fig. 5 and Table 2 of the same paper (from which we took the air case B) show a consistent drop even in the case of pure oxygen. It is evident that for this last preparation other causes of non-linearity (as, e.g. non-linear Ohmic phenomena) have to be taken into account. To verify this hypothesis, we added the non-linear fall of the pure oxygen to the fitting curve for air: we observe that, by this procedure, N_d drops to a value around 4 (well inside the expected range) in the case of 1/3 and 1/5 atm pressures, while it stays very high in the case of 1/1 atm pressures.

4.3. Comparisons with published mechanistic models

In this new light, it is also relevant to review other models found in the literature. Because all of the model examined suppose an uniform reactive region, the only characteristic length is its thickness and we may have for N_d values of 0 or 1 (see Table 1 homogeneous case). Some of the authors (Amphlett et al. [4,5], Mann et al. [6], Kulikovsky et al. [12,13], Garau [14]) assume oxygen diffusion in gas-phase; in this case, even at high current density, oxygen reaches the whole reactive region and we have that both N_d^0 and N_d^1 are worth 0. Other authors (Bernardi and Verbrugge [9], Rho et al. [18]) assume oxygen diffusion in liquid phase; this imply that already at low current density, oxygen did not reaches the whole reactive region and we have that both N_d^0 and N_d^1 are worth 1. Some other authors (Springer et al. [10], Marr and Li [19], Um et al. [20]) use intermediate values for oxygen diffusion coefficients; in these cases we may have that $N_d^0 = 0$ and $N_d^1 = 1$. In all of these papers, the value of γ is inside the range 0.5–1.

These values of N_d and γ imply a/b ratios in the range 0.5–2, which is considerably lower than the range shown in Table 2. This is the reason why the values and the shape of the performance curves given by these models, near the limiting current, are quantitatively wrong and qualitatively different from the experimental ones.

Only Springer et al. [10] tried to solve this discrepancy, and to reach this goal they used the ionic conductivity and the oxygen diffusion coefficient in the reactive region as fitting parameters. They observed that by using very low conductivity values, and ad hoc values for the diffusion coefficient, the modelled curves get closer to the experimental ones. This is due to the fact that when the current density increases, oxygen tends to concentrate near the interface with the gas diffuser, then protons have to travel a longer way through the reactive region, and the Ohmic losses increase more than linearly. This non-linear contribution (neglected by us due to the small thickness of the reactive region), becomes important when the proton conductivity gets very low. Springer et al. [10], justified the very low values of proton conductivity ($\sim$0.001 S/cm) by experimental measurements made at low humidification degree. However, it is very hard to believe that such conditions could exist in the cathode reactive region, where water is generated by the reaction.

We believe that the correct way to get agreement with the experimental data, is to change the diffusion model for the oxygen in the reactive cathode region in such a way that $N_d^0 = 0$ and $N_d^1 \in 1$–5. This can be achieved by supposing the existence of a small amount of gas pores in the reactive cathode region, and by taking into account both for the longitudinal (gas-phase) oxygen diffusion along the pores and for the transversal (liquid phase) oxygen diffusion inside the membrane phase [21].

5. Summary and conclusions

The presented semi-empirical derivation of a performance equation for PEMFCs is based on the observation that the strongest non-linear contributions to the cell potential drop at high current density are arising from interface phenomena happening in the cathode reactive region. The key quantity to describe such contributions appears to be the integral of the oxygen concentration over the reactive region. To evaluate such integral, oxygen propagation from the inlet gas channel trough the diffusion region of the cathode, and then inside the reactive region, has been described.

The oxygen propagation inside the diffusion region is determined by integrating the Stefan–Maxwell equations, with the assumption that both the nitrogen flux and the water concentration gradient are zero. We also assume that the gas porosity of the region is a decreasing function of the cell current density, in a way to simulate the well known flooding phenomenon of the cathode. The shape of this function has been found to be of minor importance on the characterization of flooding, while the important parameter is recognized to be the ratio between the gas porosity at zero and at limiting current densities.

Permeation of oxygen molecules inside the reactive region can be qualitatively described by comparing the distance travelled by the oxygen molecules with the characteristic length scales of the region. If the travelled distance is larger than the region length scales (such as the mean pore length or the mean pore distance) oxygen permeates the whole region. The more the travelled distance reduces, the more the oxygen permeated volume depends on the details of the geometrical structure of the reactive region, and the value of the integral of the oxygen concentration changes, too. The quantitative evaluation of such integral for two different models and for different ranges of the travelled distance, brings to an expression containing a parameter N_d which characterizes the structure of the reactive region.

The final empirical equation for the performance curve looks similar to other published equations (see, e.g. Squadrito et al. [3]), but in our case all equation parameters have a clear physical origin and a clear physical meaning.

The empirical equation is then used to fit a number of experimental performance curves. All analyzed experimental data are well reproduced, especially at high current density.

The model used to derive the empirical equation, and the set of numerical values found for the fitting parameters give strong evidences of the existence of flooding phenomena inside the cathode diffusion region, and of the presence of a gas pores structure inside the cathode reactive region.

Then, the modelling of such phenomena and structures seems to be necessary in order to get a quantitative description of the performance drop at high current density of an H_2/air feed cell. This kind of modelling is being used by us within a mechanistic model based on a Bernardi and Verbrugge type of approach [7,9]. Work in this direction is in progress [21].

Acknowledgements

This work has been carried out partially with the financial contribution of the Sardinia Regional Authorities, and partially with the financial support of the Centro Ricerche Fiat, Orbassano, Italy. Centro Ricerche Fiat is also acknowledged for the permission to publish some of the presented results, since they are based on a code developed by us and owned by them.

Appendix A. Evaluation of oxygen concentration integrals

From the equation for the oxygen concentration profile, Eq. (14), the integral in Eq. (11) is written as

$$\Xi(I) = (c_{O_2}^{C_R/C_D}(I))^{\gamma} \int_{C_R} \left(1 - \frac{l}{L(I)}\right)^{\gamma} dV. \tag{A.1}$$

- Homogeneous model

  In this case, we have $dV = \sigma_C\, dl$ and the integral becomes

$$\Xi(I) = L(I)\sigma_C (c_{O_2}^{C_R/C_D}(I))^{\gamma} \int_0^1 (1-x)^{\gamma}\, dx. \tag{A.2}$$

  From Eq. (13) and because in this case $\sigma = \sigma_C$ is a constant, we get

$$\Xi(I) \propto \frac{c_{O_2}^{C_R/C_D}(I)}{I} (c_{O_2}^{C_R/C_D}(I))^{\gamma}, \tag{A.3}$$

  which is the expression reported in Table 1, second row.
- Pore gas model
  - Longitudinal limitation

    In this case, we have $dV = V_{C_R}\, dl_l/L_p$ and, by following the same steps as for the homogeneous model, we get

$$\Xi(I) \propto \frac{c_{O_2}^{C_R/C_D}(I)}{I} (c_{O_2}^{C_R/C_D}(I))^{\gamma}, \tag{A.4}$$

    which is the expression reported in Table 1, fourth row.
  - Transversal limitation

    In this case, we have $dV = 2\pi L_p(l_t + R_p)\, dl_t$, where R_p is the mean pore radius, and the integral becomes

$$\Xi(I) = 2\pi L_t^2 L_p (c_{O_2}^{C_R/C_D}(I))^{\gamma} \int_0^1 (1-x)^{\gamma} \left(x + \frac{R_p}{L_t}\right) dx. \tag{A.5}$$

    The diffusion section σ is given by the internal surface of the pores, $\sigma = 2L_{C_R}\epsilon_g\sigma_c/R_p$, which, once more, is a constant.

    In the case, where $L_t \gg R_p$, the ratio R_p/L_t inside the integral can be neglected and, we get

$$\Xi(I) \propto \left(\frac{c_{O_2}^{C_R/C_D}(I)}{I}\right)^2 (c_{O_2}^{C_R/C_D}(I))^{\gamma}, \tag{A.6}$$

    which is the expresssion reported in Table 1, fifth row.

    On the other extreme, when $L_t \ll R_p$, we can write

$$\Xi(I) \approx 2\pi L_t L_p (c_{O_2}^{C_R/C_D}(I))^{\gamma} R_p \int_0^1 (1-x)^{\gamma}\, dx \propto \frac{c_{O_2}^{C_R/C_D}(I)}{I} (c_{O_2}^{C_R/C_D}(I))^{\gamma}, \tag{A.7}$$

    which is the expression reported in Table 1, sixth row.
  - Both limitations

    In this case, we have $dV = 2\pi(l_t + R_p)\, dl_t\, dl_l$ and the integral becomes

$$\Xi(I) = 2\pi \int_0^{L_l} dl_l L_t^2 (c_{O_2}(l_l, I))^{\gamma} \int_0^1 (1-x)^{\gamma} \left(\frac{R_p}{L_t} + x\right) dx. \tag{A.8}$$

    In the case, where $L_t \gg R_p$, the integral on x becomes constant and, we have

$$\Xi(I) \propto \int_0^{L_l} dl_l L_t^2 (c_{O_2}(l_l, I))^{\gamma}. \tag{A.9}$$

The value of L_t can be estimated by using Eq. (13) and by observing that $\sigma = 2L_l L_{C_R} \epsilon_g \sigma_c / R_p L_p$ is proportional to L_l

$$L_t \propto c_{O_2}(l_l, I) \frac{L_l}{I}, \tag{A.10}$$

and, we have

$$\Xi(I) \propto \left(\frac{c_{O_2}^{C_R/C_D}(I)}{I} \right)^5 (c_{O_2}^{C_R/C_D}(I))^\gamma, \tag{A.11}$$

which is the expression reported in Table 1, seventh row.

In the case where $L_t \ll R_p$, as for Eq. (A.7), we get

$$\Xi(I) \propto \int_0^{L_l} \mathrm{d}l_l L_t (c_{O_2}(l_l, I))^\gamma, \tag{A.12}$$

and finally, we have

$$\Xi(I) \propto \left(\frac{c_{O_2}^{C_R/C_D}(I)}{I} \right)^3 (c_{O_2}^{C_R/C_D}(I))^\gamma, \tag{A.13}$$

which is the expression reported in Table 1, eighth row.

References

[1] J. Kim, S. Lee, S. Srinivasan, C. Chamberlin, J. Electrochem. Soc. 142 (1995) 2670.
[2] J. Lee, T. Lalk, A. Appleby, J. Power Sources 70 (1998) 258.
[3] G. Squadrito, G. Maggio, E. Passalacqua, F. Lufrano, A. Patti, J. Appl. Electrochem. 29 (1999) 1449.
[4] J. Amphlett, R. Baumert, R. Mann, B. Peppley, P. Roberge, J. Electrochem. Soc. 142 (1995) 1.
[5] J. Amphlett, R. Baumert, R. Mann, B. Peppley, P. Roberge, J. Electrochem. Soc. 142 (1995) 9.
[6] R. Mann, J. Amphlett, M. Hooper, H. Jensen, B. Peppley, P. Roberge, J. Power Sources 86 (2000) 173.
[7] G. Murgia, L. Pisani, M. Valentini, B. D'Aguanno, J. Electrochem. Soc., 2002, in press.
[8] D.M. Bernardi, M. Verbrugge, AIChE J. 37 (1991) 1151.
[9] D.M. Bernardi, M. Verbrugge, J. Electrochem. Soc. 139 (1992) 2477.
[10] T. Springer, M. Wilson, S. Gottesfeld, J. Electrochem. Soc. 140 (1993) 3513.
[11] T. Springer, T. Zawodzinski, S. Gottesfeld, J. Electrochem. Soc. 138 (1991) 2334.
[12] A. Kulikovsky, J. Divisek, A. Kornyshev, J. Electrochem. Soc. 146 (1999) 3981.
[13] A. Kulikovsky, J. Divisek, A. Kornyshev, J. Electrochem. Soc. 147 (2000) 953.
[14] V. Gurau, Ph.D. thesis, University of Miami, Coral Gables, Florida, 1998.
[15] V. Gurau, H. Liu, S. Kakac, AIChE J. 44 (1998) 2410.
[16] J. Ferguson, J. Fiard, R. Herbin, J. Power Soucres 58 (1996) 109.
[17] D.R. Lide, H.P.R. Frederikse, CRC Handbook of Chemistry and Physics, CRC Press, Boca Raton, FL, 1994.
[18] Y. Rho, S. Srinivasan, Y. Kho, J. Electrochem. Soc. 141 (1994) 2089.
[19] C. Marr, X. Li, J. Power Sources 77 (1999) 17.
[20] S. Um, C.-Y. Wang, K. Chen, J. Electrochem. Soc. 147 (2000) 4485.
[21] L. Pisani, G. Murgia, M. Valentini, B. D'Aguanno, J. Electrochem. Soc., 2002, in press.
[22] K. Sundmacher, K. Scott, IChemE Symp. Electrochem. Eng. (Exeter), 1999.